# An Overview of the PES Pareto Method for Decomposing Baseline Noise Sources in Hard Disk Position Error Signals

Daniel Abramovitch, Terril Hurst, and Dick Henze
Hewlett-Packard Laboratories, 1501 Page Mill Road, M/S 4U-12, Palo Alto, CA 94304 *

*Abstract*— **This paper gives an overview of the PES Pareto Method, a useful tool for identifying and eliminating key contributors to uncertainty in the Position Error Signal (PES) of a magnetic disk drive servo system [1, 2, 3]. Once identified and ranked according to their overall effect on PES, the top–ranking sources can be worked on first, either by finding ways to reduce their magnitude or by altering system components to reduce sensitivity to the contributors.**

**The PES Pareto Method is based on three ideas: (1) an understanding of how Bode's Integral Theorem [4] applies to servo system noise measurements, (2) a measurement methodology that allows for the isolation of individual noise sources, and (3) a system model that allows these sources to be recombined to simulate the drive's Position Error Signal. The method requires the measurement of frequency response functions and output power spectra for each servo system element. Each input noise spectrum can then be inferred and applied to the closed loop model to determine its effect on PES uncertainty.**

**The PES Pareto Method is illustrated by decomposing PES signals that were obtained from a hard disk drive manufactured by Hewlett-Packard Company. In this disk drive, it is discovered that the two most significant contributors to PES baseline noise are the turbulent wind flow generated by the spinning disks ("Windage") and the noise involved in the actual readback of the Position Error Signal ("Position Sensing Noise").**

## I. INTRODUCTION

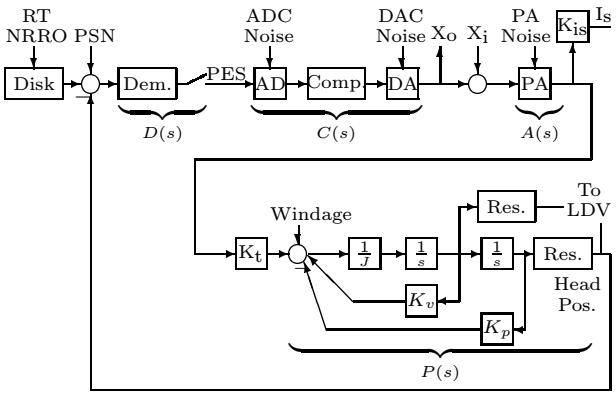


Figure 1: Generalized view of track following model.

A hard disk drive's Position Error Signal (PES) can be decomposed in the frequency domain into four components:

**External Shock and Vibrations** are heavily influenced by the drive's operating environment. It has been shown that accelerometer feedforward control can considerably reduce the effect on PES[5].

**Synchronous or Repeatable Excitations** are due to the rotation of the spindle and therefore synchronous with it or one of the spindle orders. While synchronous excitations may be large, standard practice in the disk drive industry includes using feedforward cancellers to reduce the effects of synchronous excitations [6].

**Non-synchronous or Non-repeatable Excitations** include sharp spectral peaks due to spindle bearing cage orders and structural resonances (which are less sharp but still narrow band). Recent work suggests that disturbances due to resonances or cage orders can be considerably reduced by the use of damped disk substrates and fluid bearing spindles [7].

**Broadband or Baseline Noise** is what remains when all of the narrow band components have been removed. Of the four categories, baseline noise has received the least attention in the literature. Therefore, it is the one singled out as the focus of this method.

In order to increase track densities, all sources of PES uncertainty must be reduced. There is prior work to indicate that the first three categories have been well studied, and that reasonable engineering solutions are available. This is not true for the baseline noise; therefore, of the four categories, it is the one singled out as the focus of this method. The PES Pareto Method and the measurement techniques for noise source isolation to isolate the building blocks of the PES baseline were used. The reasoning was that understanding the building blocks of the baseline noise, would allow solutions that worked on those building blocks.

The purpose of this paper is to give an overview of the PES Pareto Method, a method of breaking down the Position Error Signal (PES) of a magnetic disk drive to its contributing components. A more detailed treatment geared primarily towards the control/servo community can be found in [1, 2, 3]. This treatment is intended to introduce the method to the magnetic storage community.

## II. MEASUREMENT OVERVIEW

In order to guide our measurements and our modeling, it is useful to have a map of the system. The block diagram in Figure 1 will serve as the map for our tour of noises in the system. Starting at the left of this diagram, the reference position that the actuator arm must follow is the position of the magnetic track written on a disk, turning on a spindle. Only the position error – the difference between the reference track position and the readback head position – is sensed by the readback

*Manuscript received June 16, 1997. E-mail: D. Abramovitch (danny@hpl.hp.com), T. Hurst (terril@hpl.hp.com), D. Henze (Dick_Henze@hpl.hp.com).

head, and this error signal is sent to the demodulator. The demodulator outputs a set of numbers at the system sample rate, and these are combined electronically to form PES. This PES signal is then converted to a digital format via an analog to digital converter (ADC), filtered by the compensator and then sent back out to the power amplifier via a digital to analog converter (DAC). The power amp converts the desired voltage into a current to drive the voice coil actuator (with torque constant $K_t$). The actuator itself has rigid body behavior as well as resonances. Through this, the head position is set. The position error is then sensed by the head. Absolute head position is not generally known from what is read off of the disk surface, but can be obtained in the laboratory by shining a laser spot from a Laser Doppler Vibrometer (LDV; in this case, made by Polytec) off of the side of the head. While this nominally measures velocities, the result can be accurately integrated in time (for the frequencies we are concerned with) to obtain position.

There are several measurement points that can be accessed around the loop: $X_o$, $I_s$, PES, and head velocity (and position) via the LDV. Test signals can usually be injected into the loop only at $X_i$. These are shown in Figure 1.

There are several likely noise input points on a disk drive. First of all, there are the noises associated with the moving disk and the readback process. These all enter the loop at the same point, but have different root causes. The noise due to the motion of the disk attached to a ball bearing spindle creates both Repeatable Run Out (RRO) (typically at orders of the spindle rotational frequency) and Non-Repeatable Run Out (NRRO). One of the interesting properties of servowritten disks is that one pass of the NRRO is usually locked into the servo position information when it is written. Thus, this written in NRRO is repeated at every revolution of the disk. The other noise source that enters at this point is the noise from the readback process of position information, called Position Sensing Noise (PSN). This noise can be due to the magnetic domains on the disk, the behavior of the magnetic readback head, the interaction of these two, or the action of the demodulator. (We lump demodulator noise into PSN for our current analysis.) Downstream in the loop, there are potential noise sources at the ADC and DAC (due to quantization), noise at the power amp, and finally Windage. Windage is caused by the air flow generated as the disk spins. This air flows over, under, around, and into the actuator arms and the readback head, disturbing the head position.

The tools available to us are a set of laboratory instruments that can make both time and frequency domain measurements. In particular, Digital Storage Oscilloscopes (DSO) can record time domain data as can certain spectrum analyzers. The spectrum analyzers are most useful, though, for measuring linear spectra, power spectra, power spectral densities (PSDs), and frequency response functions of systems. In particular, the spectrum analyzers that we use are the HP 3563A Control Systems Analyzer and the HP 3567A Multi-Channel Analyzer. The latter instrument has the advantage of allowing more than two signals from the system to be measured at once.

For analysis, we have the standard set of matrix based tools. In particular, we are using Matlab and Simulink. (Note that we will use these terms generically, allowing the reader to substitute their favorite controls CAD software package.) As has been the practice in our laboratory for several years, the measurements are made with a conscious thought of transferring them into Matlab/Simulink for analysis[8].

Given these tools, there are three types of measurements on which we could base our analysis: power spectra, linear spectra, and time domain measurements. The specific tradeoffs involved in choosing one of these are discussed in [1]. For reasons mentioned there, power spectra (or PSD's, displayed in power spectral density units) appear to be the most promising measurements. All frequency response function (FRF) and power spectral density (PSD) data must be taken over the same bandwidth and with the same resolution (10-6410 Hz and 2 Hz, respectively, in this case).

## III. BODE'S THEOREM ON SENSITIVITY FUNCTIONS

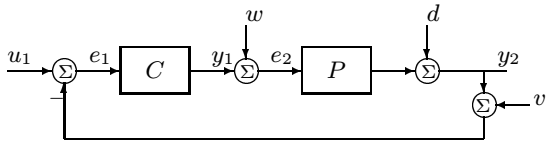


Figure 2: Block diagram of closed-loop system.

There is is an old theorem by Bode [4] which deals with what he calls regeneration. It turns out that this theorem has some very interesting applications to control systems.

### A. Sensitivity Functions

The sensitivity function, $S$, is also known as the disturbance rejection function because it shows how disturbances, $d$, go through the system and show up at the output, $y$, or at the error signal $e$.

$$S = \frac{e_1}{u_1} = \frac{1}{1+PC} = \frac{y_2}{d} = -\frac{e_1}{d}. \tag{1}$$

### B. Bode's Integral Theorem

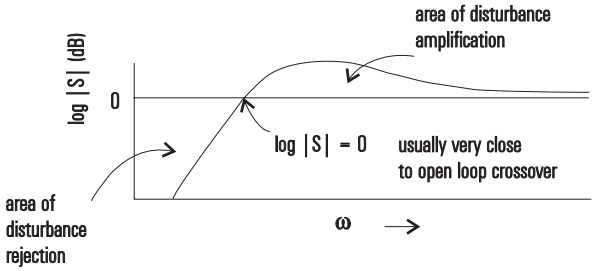


Figure 3: Sensitivity function.

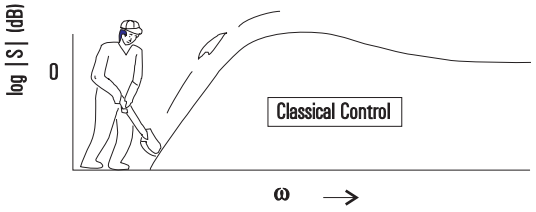


Figure 4: Stein's depiction of classical control.

While the mathematics used to prove both versions of Bode's Theorem can be fairly complicated, the result is fairly simple and extremely powerful. We will leave the proofs to the references [4], [9] and talk simply about the interpretation. Looking at Figure 3 it says simply that:

$$\begin{array}{c}\text{the area of}\\ \text{disturbance}\\ \text{amplification}\end{array} = \begin{array}{c}\text{the area of}\\ \text{disturbance}\\ \text{rejection}\end{array} + \begin{array}{c}\text{a non-}\\ \text{negative}\\ \text{constant.}\end{array} \tag{2}$$

Mathematically, this is stated as

$$\int_0^\infty \log|S| d\omega = c, \tag{3}$$

where $c$ is some positive constant dependent only on the open loop unstable poles and non-minimum phase zeros.

Consequences: "Sooner or later, you must answer for every good deed." (Eli Wallach in the *The Magnificent Seven*)

Translation: If you make the system less sensitive to noise at some frequencies, you then make the system more sensitive at other frequencies.

Typical control designs attempt to spread the increased sensitivity (noise amplification) over the high frequencies where noise and/or disturbances may be less of an issue. The image of this was provided in the Bode Lecture at the 1989 IEEE Conference on Decision and Control (Tampa, FL)[10]. The talk, by then Honeywell Researcher and MIT Professor, Gunter Stein, was entitled "Respect the Unstable." Stein described the net effect of control systems design as trying to get a certain amount of disturbance rejection at some frequency span while trying to thinly spread the amplification over a large frequency span. Stein's drawing had a guy shoveling disturbance amplification "dirt" as in Figure 4. The dirt can be moved, but not eliminated. Furthermore, the discrete-time version of Bode's Integral Theorem [9] has some implications for discrete time systems [1], however they are essentially those of the continuous time theorem with the Nyquist rate forming a retaining wall for the disturbance amplification dirt.

There are two reasons why Bode's Integral Theorem is important in a discussion of a disk drive's Position Error Signal. First of all, it gives a very good gauge on what can and cannot be done with disturbance rejection and noise in a control system. An intelligently designed control system puts noise amplification in places where there is little noise. A poorly designed system results in significant noise amplification.

The second reason will become apparent in the next section. It turns out that when PES is measured from a closed loop system, the loop should actually be opened up to look at PES. The *exact same effects* that are the point of the above theorem affect a measurement of PES.

## IV. PES MEASUREMENTS AND LOOP UNWRAPPING

Typically in a disk drive the Position Error Signal (PES) is only measured in closed-loop. This is in general due to the difficulties of obtaining a linear measurement of head position across multiple tracks while the loop is not closed. What seems less common is "opening the loop" as is often done with closed-loop transfer function measurements. While a PSD of closed-loop PES might be a reasonable measure of loop performance, it is not the useful quantity for determining what the noise *inputs* to the system are. In order to obtain this quantity, we want to open the loop, either physically or mathematically.

Referring back to the block diagram in Figure 2, the sensitivity function, which is also the transfer function from $u_1$ to $e_1 (= PES)$, is given in Equation 1. We typically think of the sensitivity function as the error response, $e_1$, from either the reference, $u_1$, or a disturbance, $d$. It can be obtained by measuring the closed-loop response from $w$ $(X_i)$ to $y_1$ $(X_o)$ $\left(= T = \frac{PC}{1+PC}\right)$ and subtracting $T$ from 1 *i.e.,* $S = 1 - T = \frac{1}{1+PC}$.

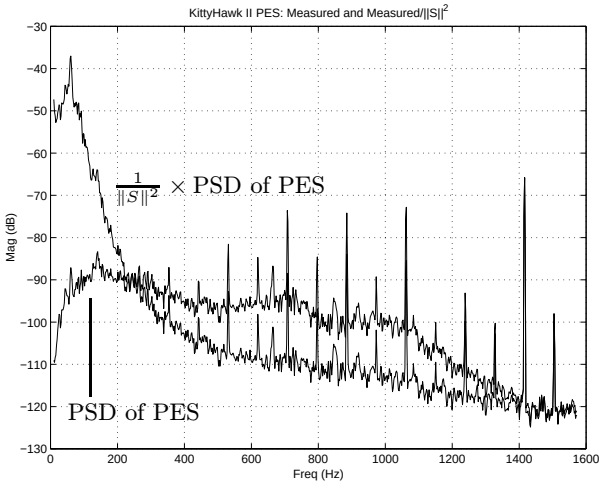


Figure 5: PSD of PES, and PSD of PES filtered by $\frac{1}{|S|^2}$.

Note that while the PSD of PES is typically measured as a closed loop quantity, we are now in a position to extract the input to the loop that would yield that PES PSD. Since the transfer function from $u_1$ to $e_1$ is given by $S$, a noise PSD input at $u_1$ would be filtered by $\|S\|^2$ by the time it showed up at $e_1$. Thus, if we start with a measurement of noise at $e_1$, we can filter backwards by $\frac{1}{\|S\|^2} = \|1 + PC\|^2$ to get the input at $u_1$ that could have generated it. The procedure above shows how to measure the exact filters needed to "open" the loop.

Figure 5 shows the PSD of PES as measured and when filtered by $\frac{1}{\|S\|^2}$. In the context of Bode's Integral Theorem, the plot makes complete sense. The measured PES only looks flat because of the action of the feedback loop. In fact, the "open-loop" plot of the PES PSD can be approached by lowering the loop gain until the system is barely track following. At that point, the closed-loop PES PSD will look very much like the "opened-loop" PES PSD, because the effect of the feedback loop will have been minimized. The effect of the feedback loop is to push disturbances down at low frequency while amplifying them at high frequency.

## V. THE PES PARETO METHOD

Given that we have the elements to construct the appropriate filters, there is a common theme for each noise source:

- Isolate a measurement of a noise source.
- Filter backwards from the measurement point to the noise input to obtain the noise source input PSD.
- Filter forwards from the noise source input to PES to obtain the effect of this noise on the PES PSD.
- Compare the PSDs at PES and add to cumulative PES PSD.
- Integrate across frequencies to obtain power spectra and total variances for each noise source.

As simple as this methodology might seem, it can yield surprisingly profound results. The net result is to identify which noise sources in a disk drive are truly limiting the servo performance. The following section will offer an example of this

method in the specific case of a magnetic disk drive made by Hewlett-Packard.

## VI. MEASUREMENTS FOR PES PARETO

In order to do the appropriate filtering, certain frequency response functions need to be either generated from a model or measured in the laboratory. Since we are filtering PSDs, the operation will involve the magnitude squared of the filter response.

The closed loop frequency response function can be directly measured, as can the compensator, and "mechanics" frequency response functions[2]. As noted earlier, these measurements are essential to deriving the appropriate filters of the relevant noise PSDs.

The following power spectra were obtained from each of the measurement points illustrated in Figure 1, with system parameters being varied in order to assess the system's sensitivity to each noise source. We present these power spectra in the order suggested by the system diagram, beginning with PES and ending with estimates of Position Sensing Noise (PSN). The analysis of PSN is presented last, because it relies on a different type of measurement and analysis than the other noises.

The full set of power spectra are presented in [2]. Detailed discussion of how this data is used in the PES Pareto method is given in [3]. The data presented here has been filtered to remove synchronous spectral lines, since we were interested primarily in the PES broadband baseline effects.

### A. DAC and ADC Resolution

One suggested source of PES uncertainty is the finite resolution of the digital–to–analog (DAC) and analog–to–digital (ADC) converters on either side of the compensator. The starting point for determining this uncertainty was to successively mask off bits of each converter and observe changes in the PES power spectrum. This was accomplished by colleagues at HP's Disk Memory Division[2]. These spectra were later subtracted from each other in order to isolate quantization noise [3].

### B. Slider and PES Spectra

Figure 6 illustrates the effect of loop gain on the spectra of PES and radial slider displacement. PES and LDV velocity were measured with (1) standard loop gain, (2) loop gain programmatically set to zero, and (3) the actuator physically disconnected from the servo system. In addition to the elimination of spectral lines mentioned previously, the presence of a LDV setup resonance (approximately 700 Hz) and the known disk resonances (500–1200 Hz [11]) required further smoothing of this data when performing the PES decomposition.

By measuring LDV and PES spectra under these loop conditions, we were able to estimate power amplifier noise (the difference between open–actuator and zero–gain measurements) and airflow or "Windage" (open–actuator response).

Figure 7 is a series of radial slider displacement power spectra which were obtained at different rotational speeds ranging from 3600 to 9600 RPM with the loop open. Again, the 700 Hz LDV setup resonance is shown (and eventually removed from the data). A series of flexure resonances are also shown between 5—6 kHz.

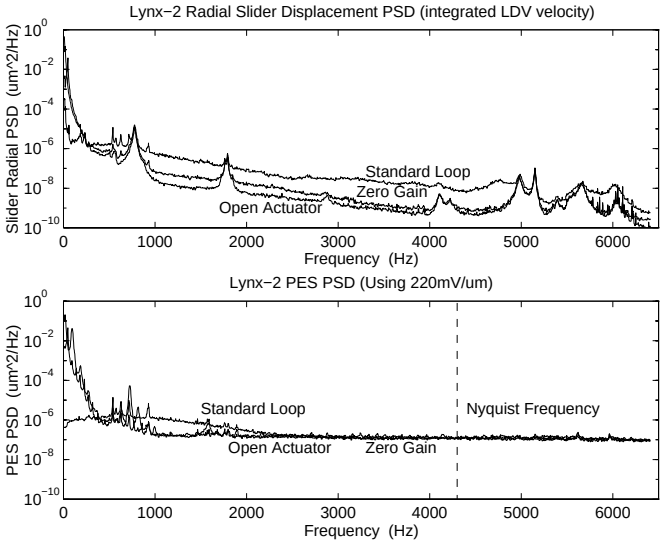


Figure 6: Radial Slider and PES Spectra vs. Loop Gain.

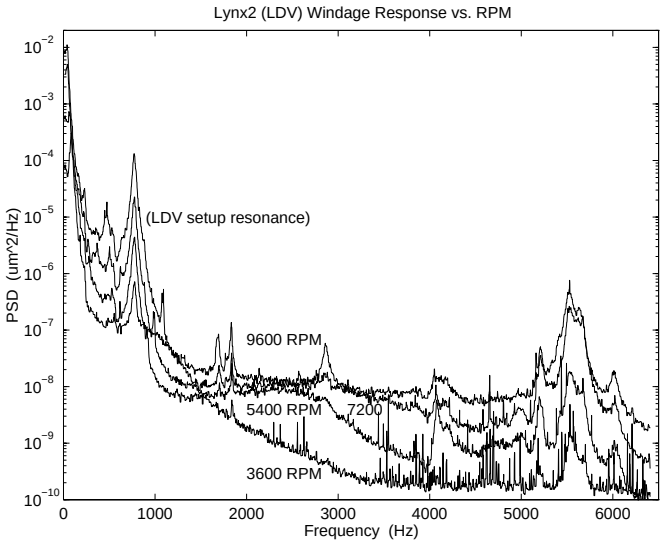


Figure 7: Radial Slider Movement vs. RPM.

### C. Position Sensing Noise

We now consider the final noise source: Position Sensing Noise (PSN). PSN is the error resulting from the process of magnetically sensing and electronically demodulating position information. We perform a statistical two–way *analysis of variance* (ANOVA) on the demodulated servo signal. Computational details for ANOVA are described in [12]. This paper reports results for a dedicated–servo case, but the method was originally developed for a sectored-servo disk drive. Differences in how to apply ANOVA for the two cases are described below.

*1) ANOVA Description and Method* The ANOVA method partitions statistical variations between error due to actual displacement and error due to PSN. In order to perform this analysis, we assume zero displacement across a set of $n$ servo bits during a single servo burst observation. This seems plausible, given the relatively low frequencies of mechanical motion (less than 10 kHz) and short servo data window (less than 20 microseconds). Thus, bit–to–bit variations within an observed servo burst will be assumed to be completely due to

position sensing uncertainty.

Samples of size $n$ are selected from each of $k$ populations (each sample is from the same servo burst, observed at $k$ different times). In the sectored–servo case, the natural value of $n$ is the number of servo bits within a given sector; for the dedicated–servo case, the number chosen is somewhat arbitrary—short enough to insure the zero–displacement assumption described above, but long enough to provide statistically significant variability. In the dedicated–servo case reported here, $n = 18$ and $k = 32$, yielding $18 \times 32 - 1 = 575$ statistical degrees of freedom. Values for each ensemble of $n$ bits result from different *treatments*, which are not under our direct control, but rather, applied by the servo system as it attempts to follow track center. Treatments and measurement error are both assumed to be random and mutually independent.

The response for each servo bit is written as

$$Y_{ij} = \mu + \Delta_i + E_{ij} \ ; \quad i = 1, 2, \ \ldots \ k, j = 1, 2 \ \ldots \ n. \qquad (4)$$

The right–side components of Equation 4 are $\mu$, the mean value of PES; $\Delta_i$, the effect due to random displacement error (the "treatment"); and $E_{ij}$, the effect due to measurement error. Both $\Delta_i$ and $E_{ij}$ are assumed to be normally distributed around a zero mean. The *variance* of $\Delta_i$ is $\sigma^2_\Delta$, and the variance of $E_{ij}$ is $\sigma^2_Y$; both are computed from the collected data set of length $n \ \times \ k$ in accordance with the ANOVA method.

The variance of PSN, $\sigma^2_s$, depends on how the individual servo bits are processed, which is different for sectored– and dedicated–servo cases. Again, relying on the independence assumption, the sectored-servo PSN variance is based on pair–wise subtraction of bits A and B, $Y_A - Y_B$, i.e.,

$$\sigma^2_s = \frac{\sigma^2_A}{n} + \frac{\sigma^2_B}{n} \quad (sectored) \qquad (5)$$

For the dedicated–servo case, $\sigma_s$ is computed in the following manner:

- Digitize several samples (at least 30) of the servo waveform
- Mathematically peak–detect the servo bit values.
- Use the ANOVA procedure to estimate the per–bit variance in position sensing, $\sigma_Y$ .
- Mathematically generate a Gaussian noise time sequence $X(t)$ , using $\sigma_Y$ and a random number generator.
- Low-pass filter $X(t)$ by the servo demodulation filter:
  - $G(s) = \frac{10^{10}}{As^3 \ + \ Bs^2 \ + \ Cs^5 \ + \ D}$ ;
  - $Z(t) \ = \ lsim(\ G(s), X(t), t\ )$ ;

*lsim* is a Matlab linear system simulator routine; For the current servo system, $A = 8.61 \times 10^7$, $B = 3.95 \times 10^{-1}$, $C = 1.49 \times 10^5$, and $D = 10^{10}$. The resultant $\sigma^2_s$ of $Z(t)$ is an estimate of PSN.

*2) Test Results* We obtained separate PSN estimates for the dedicated–servo A– and B– bits: $\sigma^2_A = 0.264\ \mu m^2$ and $\sigma^2_B = 0.275\ \mu m^2$. Therefore, a mid–range value of $0.269\ \mu m^2$ is used for $\sigma^2_Y$. This value was used in the procedure outlined above to obtain a value for PSN of $\sigma_s = 0.0295$ microns, which closely matches the predicted value obtained from the PES Pareto decomposition.

### *D. Measurement Summary*

The measurements described above are accomplished by connecting to test points which are typically available for all disk drive products in the normal development process. The idea is to isolate each component of the servo system by making measurements on either side—where possible—or, as the case for Position Sensing Noise, collect data and analyze it under a set of reasonable assumptions (i.e. white noise). With this data in hand, it is possible to complete the third step in the PES Pareto method, namely, determining the effects of individual noise contributors on PES [3]. Thus, the collection of required data is accomplished in a fairly straightforward manner, assuming care is taken to take sufficient, high–quality measurements.

## VII. THE STRATA OF PES

> When you have eliminated the impossible, whatever remains, *however improbable*, must be the truth.
> — *Sherlock Holmes[13]*

The above quotation holds in it the key philosophy of the PES Pareto Method: eliminate all the impossible, observe what is left, and from there determine the true sources of noise in a disk drive's Position Error Signal (PES). The preceding description has shown a method for separating the contributors of various sources of uncertainty ("noises") in the position error signal (PES) of the track-follow servo in a disk drive and how specific measurements are made to isolate individual noise sources and to create appropriate filters from which the noises can be examined at their source and at PES. This section completes the process by using the method and the measurements to feed the appropriate spectra through the appropriate loop filters to yield both the input noise spectra and their effect – both individually and cumulatively – on PES. The PSDs are then integrated in frequency to yield the corresponding power spectra and variances. Due to space constraints, the discussion of backward filtering individual noise measurements to their source input and forward filtering these to PES is left in [3]. This section will show the strata as it appears at PES.

Given that several of the individual noise sources and their effects on PES have been identified, they can now be compared individually or stacked up cumulatively as shown in Figure 8. (The latter is shown since the stacking of the PSDs and variances makes is more readable than lines which criss-cross.)

Note that even though most of the potential sources shown in the small block diagram of Figure 1 and described in detail in the method paper[1] have been accounted for, there is still a significant portion of the baseline PES PSD that is unaccounted for, especially at high frequencies. This is especially obvious in the cumulative variance plot in Figure 8. If one zooms in on the total baseline PES PSD and subtracts off what has been accounted for, one gets a curve which very much looks like a scaled version of $\|D(s)S_{cl}(s)\|^2$ *i.e.,* the squared magnitude of the transfer function from the reference input to PES, as shown in [3]. This suggests a noise which is injected at the reference input, and the two possibilities here for

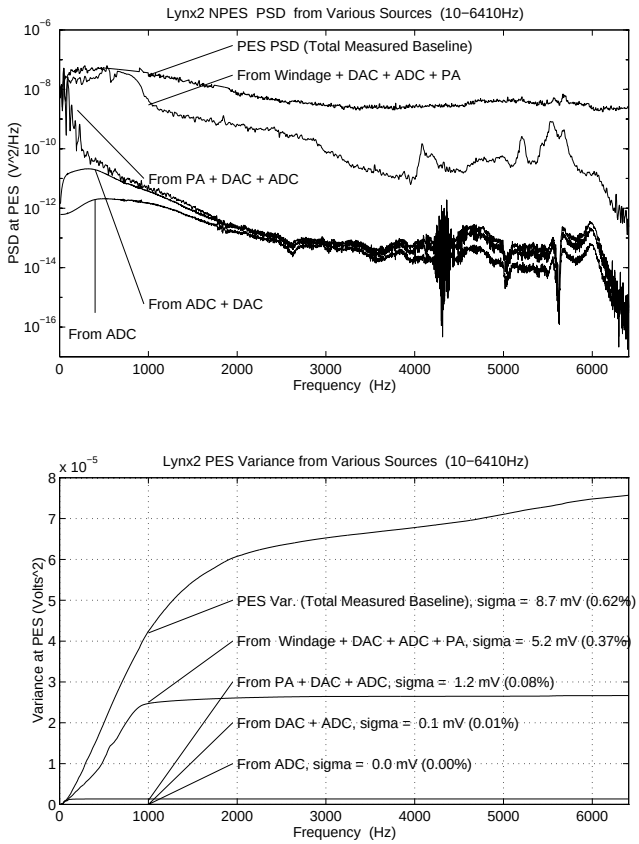


Figure 8: Cumulative Noise Source PSDs at PES

non-repeatable baseline noise are Real Time Non-Repeatable Run Out (RT NRRO) and Position Sensing Noise (PSN). By filtering the "what's left" curve back to the input by

$$\left\| \frac{1}{D(s)S_{cl}(s)} \right\|^2$$

a very interesting result drops out as shown in Figure 9. Note that there is a broadband, essentially white noise component to "what's left". There is also a large hump at low frequency. As Windage is accounted for already, the most likely source of this large hump is the actual non-repeatable motion of the disk on the rotating spindle (RT-NRRO). Likewise the broadband flat noise cannot be from the power amplifier, ADC, or DAC (since these have been eliminated) and therefore it follows that this is Position Sensing Noise. If this PSD is fed forward to PES and then integrated in frequency to yield the PES baseline variance due to PSN, this number, $\sigma_{PSN} = 0.03\mu m$, closely matches the prediction of the ANOVA analysis (see Subsubsection 2)).

## VIII. EXTRAPOLATIONS

At this point, we have made use of all of our measurements and must now do some deduction from what is left. If in fact, the PSN is white, then we can extrapolate back from the flat portion of the curve in Figure 9. Calling this PSN, we can then subtract this value from the "what's left" input PSD to obtain the PSD of the Real Time NRRO.

Given that we have isolated the "white" PSN input, we can now do some modeling experiments where we alter the level of the PSN to observe the effect on the overall level of baseline PES. With the spindle rotating at the nominal speed of 5400 rpm, the results are shown in Figure 10.

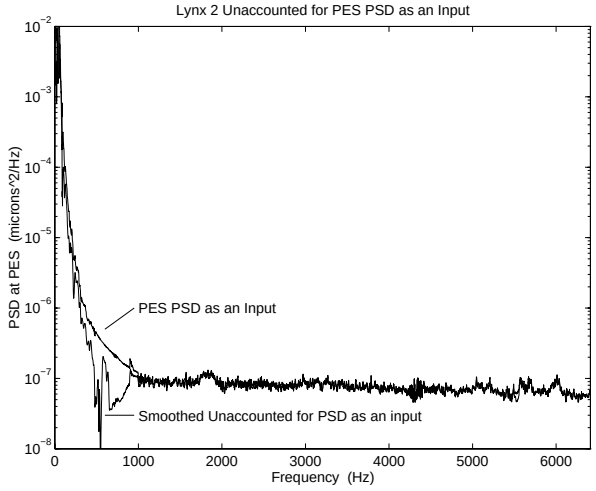


Figure 9: Unaccounted PES Noise as an Input

Likewise, having isolated Windage's contribution allows us to examine the effect of increased Windage on the overall PES baseline. As Windage was something we could actually measure, the spindle speed was adjusted using a special spindle controller board to allow measurement of Windage for spindle speeds of 3600, 5400, 7200, and 9600 RPM. The measurement results are shown in Figure 7. The procedure for feeding these Windage PSDs back to the source and forward to PES is identical to what has been done at the nominal spindle speed of 5400 RPM. It is useful to look at the overall PES variance due to Windage with changing RPM, and this is shown in Figure 11. Note that the increase in baseline PES variance is *not* linear with spindle speed, but in fact grows dramatically at the higher RPMs. This is significant as newer high performance drives spin at 7200 RPM and beyond.

## IX. CONCLUSIONS

What should be apparent now is that in this particular disk drive, there are two main sources of baseline noise in PES. The first is Windage, which is responsible for approximately one third of the total measured baseline PES variance. Windage has an effect primarily at low frequency (below 1 KHz). The second major contributor is Position Sensing Noise (PSN). PSN is flat at the input, but is shaped by the loop so that it has a rapid ramp up at low frequency and then tapers to a constant level at high frequency. However, because of the broadband nature of this noise, its effect dominates the higher frequencies (above 1 kHz).

Furthermore, these noises are tied together through the loop behavior in a way described by Bode's Integral Theorem [4]. Any attempt to drive down the PES variance caused by Windage through increased loop bandwidth results in an amplification of PSN by the loop. Minimizing the bandwidth so as not to amplify PSN probably means that the Windage is not adequately attenuated. The situation only gets worse as the spindle RPM goes up, driving up the level of Windage and therefore requiring more loop bandwidth. This greater bandwidth *must* increase the amplification of PSN.

In this context, it becomes clear that two distinct efforts will yield a lower baseline PSD for PES. The first effort is to carefully study the wind flow within a disk drive to find ways to minimize the level of Windage noise. This is a nontrivial task involving the study of turbulent air flows [14]. The

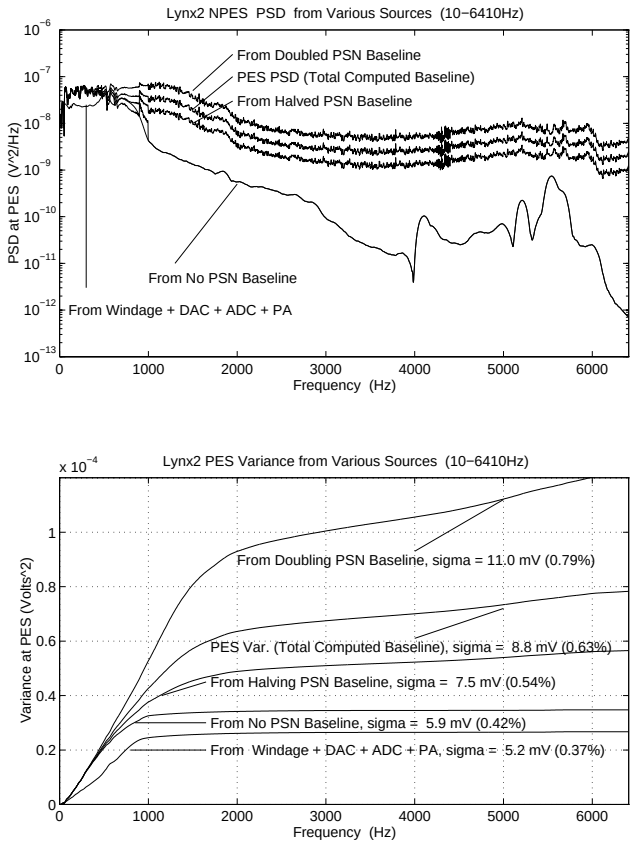


Figure 10: Effect of Changing Baseline PSN (5400 rpm)

second effort is to find ways to minimize PSN. This can be accomplished via improving the readback process and/or the demodulation process. Research is currently being done on the latter [15], [16]. It is possible that the best answer might require an entirely new position sensing method. Recognizing the significant effect that PSN has on overall baseline PES allows us to justify such an effort.

## REFERENCES


[1] D. Abramovitch, T. Hurst, and D. Henze, "The PES Pareto Method: Uncovering the strata of position error signals in disk drives," in *Proceedings of the 1997 American Control Conference*, (Albuquerque, NM), AACC, IEEE, June 1997.

[2] T. Hurst, D. Abramovitch, and D. Henze, "Measurements for the PES Pareto Method of identifying contributors to disk drive servo system errors," in *Proceedings of the 1997 American Control Conference*, (Albuquerque, NM), AACC, IEEE, June 1997.

[3] D. Abramovitch, T. Hurst, and D. Henze, "Decomposition of baseline noise sources in hard disk position error signals using the PES Pareto Method," in *Proceedings of the 1997 American Control Conference*, (Albuquerque, NM), AACC, IEEE, June 1997.

[4] H. W. Bode, *Network Analysis and Feedback Amplifier Design.* New York: Van Nostrand, 1945.

[5] D. Abramovitch, "Rejecting rotational disturbances on small disk drives using rotational accelerometers," in *Proceedings of the 1996 IFAC World Congress*, (San Francisco, CA), pp. 483–488 (Volume O), IFAC, IEEE, July 1996.


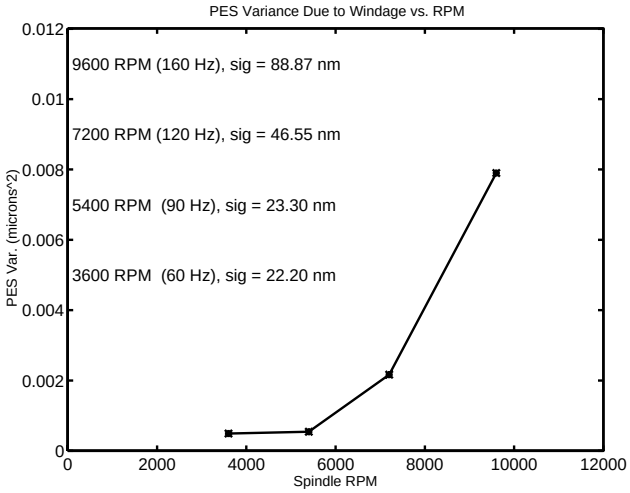


Figure 11: PES Variance Due to Windage Versus RPM


[6] A. Sacks, M. Bodson, and W. Messner, "Advanced methods for repeatable runout compensation (disc drives)," *IEEE Transactions on Magnetics*, vol. 31, August 1994.

[7] J. S. McAllister, "Disk flutter: Causes and potential cures," *Data Storage*, vol. 4, pp. 29–34, May/June 1997.

[8] D. Y. Abramovitch, "The Banshee Multivariable Workstation: A tool for disk drive research," in *Advances in Information Storage Systems, Vol. 5* (B. Bhushan, ed.), pp. 59–72, ASME Press, 1993. ISBN 0-7918-0031-8.

[9] C. Mohtadi, "Bode's integral theorem for discrete-time systems," *Proceedings of the IEE*, vol. 137, pp. 57–66, March 1990.

[10] G. Stein, "Respect the unstable." Bode Lecture presented at the 1989 IEEE Conference on Decision and Control, Tampa FL, December 1989.

[11] J. S. McAllister, "The effect of disk platter resonances on track misregistration in 3.5 inch disk drives," *IEEE Transactions on Magnetics*, vol. 32, pp. 1762–1766, May 1996.

[12] R. E. Walpole and R. H. Myers, *Probability and Statistics for Engineers and Scientists.* New York, NY: Macmillan, second ed., 1972.

[13] S. A. C. Doyle, *The Sign of Four.* 1890.

[14] H. Suzuki and J. A. C. Humphrey, "Flow past large obstructions between corotating disks in fixed cylindrical enclosures," in *Proceedings of the ASME IMECE Conference*, (Atlanta, GA), ASME, August 1996.

[15] A. H. Sacks, "Position signal generation in magnetic disk drives," Ph.D. Thesis, Carnegie Mellon University, DSSC, Department of Electrical and Computer Engineering, Carnegie Mellon University, Pittsburg, PA 15213-3890, September 5, 1995.

[16] P. Mathur, "Position signal generation on magnetic disc drives." Ph.D. Thesis Proposal at CMU, May 1996.